The Pivotal Role of Critical Hydroxyl Concentration in Si-Rich Zeolites for Switching Vapor Adsorption

M. Lions, Cécile Daniel, B. Coasne, Frédéric Meunier, A. Tuel, D. Farrusseng

The Pivotal Role of Critical Hydroxyl Concentration in Si-rich zeolites For Switching Vapor Adsorption

Mathieu Lions[†], Cécile Daniel[†], Benoit Coasne[‡], Frederic Meunier[†], Alain Tuel[†], David Farrusseng[†,*]

[†] Université de Lyon, Université Claude Bernard Lyon 1, CNRS, IRCELYON, Villeurbanne, France

[‡] Univ. Grenoble Alpes, CNRS, LIPhy, 38000 Grenoble, France

* To whom correspondence should be addressed: David Farrusseng

Email: david.farrusseng@ircelyon.univ-lyon1.fr

Abstract. The design of efficient separation and catalytic processes in nanoporous adsorbents requires to finely tune gas adsorption in their porosity. Here, using a large set of Si-rich zeolites (Silicalite-1, Beta, Chabazite, ITQ-13), we report on an experimental study of vapor adsorption in zeolites showing the pivotal role of the hydroxyl concentration. By studying the adsorption of water and methanol in zeolites assisted with in situ IR and ^{29}Si NMR measurements, we find that adsorption switches from non-wetting to wetting as the hydroxyl surface density reaches the same critical value ~2.5 OH/nm^2. While this hydroxyl concentration-induced crossover is well-known for water, we extend here the concept of a critical concentration by showing that a consistent picture arises when different polar substrates are considered. In particular, by establishing a generic behavior between the two protic substrates (H_2O, MeOH), we pave the way for the rational design of hydrophobic adsorbents.

INTRODUCTION

The properties of confined water but also other polar molecules such as methanol and ethanol in subnanometric cavities – the so-called angstropores – is an important issue in many areas of science and technology [1,2]. The special case of water confined in hydrophobic cavities, especially in hydrophobic zeolites such as dealuminated zeolites (Y, EMT), Si-rich BEA and ZSM-5, and all-silica zeolites (Silicalite-1, Beta), remains a topic of fundamental and applied relevance [3]. In addition, with more and more separation and catalytic processes to design, understanding the competing adsorption behavior for other molecules is becoming urgently needed. In this context, understanding the changes in adsorbate molecule properties due to its interactions with a hydrophobic substrate is relevant to many application fields such as molecular spring [4,5], alcohol-water separation [6], waste water treatments [7,8], COV capture [9] and catalytic epoxidation [10]. In the specific context of water in nanoporous media, the thermodynamics of capillary evaporation and/or intrusion in hydrophobic environments has been considered in detail using both experimental and molecular simulation [3, 11–13]. More recently, by considering several adsorbent/adsorbate couples, adsorption was found to display reminiscent capillarity [14] even when the pore size is much lower than the critical pore diameter below which pore filling becomes reversible and continuous [15]. Yet, despite such available frameworks to describe gas adsorption in extreme confinement, the estimation at which gas filling (or emptying) occurs remains a complex challenge as structural defects in zeolites – whose nature and concentration depend of the synthesis process – largely impact and even prevail in the thermodynamics at play.

The chemistry of zeolitic defects – including its zoology (e.g. type, density) and impact on surface adsorption (e.g. hydrophobicity/philicity) has been intensively studied [6, 11, 16–20]. Defective sites “Si–OH” in zeolites are classified as follows: (a) Si–O- defects (siloxy groups) which counterbalance the charge of cations for Al-containing zeolites such as ZSM-5 or partially dealuminated zeolites, (b) Si–OH defects formed from Si–O–Si bridges via hydrolysis, (c) Si–OH groups generated by missing tetrahedral framework atoms (T vacancies) coined as “silanol nest” defects, (d) Si–OH groups due to a stacking disorder, and (e) Si–OH groups at the external surface [21]. These defects interact with water, and once the number of water molecules in the cavities is increased, water clusters are formed through hydrogen bonding. All of these defect types can possibly coexist in as-synthesized zeolites and post-synthesis treated zeolites (e.g. dealumination). For Si-rich zeolites, the strongly hydrophilic Al sites are the source of water attraction, while for all-silica zeolite (e.g silicalite-1) it is well-known that a substantial number of internal defects in the form of silanol groups can form in basic synthesis conditions [17, 21, 22]. The polar nature of these silanol groups makes the zeolite more hydrophilic than

expected. On the other hand, zeolites prepared in fluoride (F^-) medium show significantly lower concentration of internal silanol defects [23–26].

In contrast to films and surfaces, for which wetting (i.e. hydrophilicity) can be estimated by contact angle measurements, there is no unique method and even less a unique wettability scale for nanoporous materials. Advantages and drawbacks of proposed methods and associated hydrophobicity indexes have been critically reviewed by Gläser [27]. For the fine characterization of surface-adsorbate interactions, avoiding as much as possible the impact of adsorbate-adsorbate interactions, adsorption isotherms in the low pressure – typically, the Henry regime where adsorbed amount increases linearly with pressure – is the most appropriate technique. In particular, from low pressure adsorption isotherms, adsorption (Henry) constant and heat of adsorption at vanishingly small coverage can be estimated. In the specific case of water adsorption, there is an abundant literature on the nature and concentration of Si–OH defect sites and its impact on the hydrophobic to hydrophilic transition in zeolites. Of particular relevance, by means of Monte Carlo simulations, it was found that the presence of 0.125 silanol nest per unit cell in silicalite-1 increases significantly the heat of adsorption at low coverage while the additional water uptake is almost insignificantly [28]. On amorphous silica film, a hydrophobic-hydrophilic transition has been estimated for a silanol concentration of 3.7 Si-OH/nm^2. While the concept of a critical hydroxyl concentration to induce hydrophilicity is rather intuitive, there is to date no simple rationalization of its value. The situation is even more puzzling as data are reported either in surface density (typically, for films and non-porous surfaces) or volume density (dense and porous materials). Even for a given nanoporous material type – e.g. zeolites – there is to the best of our knowledge no model to predict the critical hydroxyl concentration above which the non-wetting/wetting crossover is observed. Last but not least, while the impact of such defects on water adsorption and the underlying concept of hydrophobicity/hydrophilicity has been investigated, its extension to other dipolar fluids to establish a generic picture of such crossover in nanoporous adsorbents is still lacking.

To address these central questions, we report here an experimental study to assess the critical OH concentration below which silica-rich and all silica-zeolites remains non-wetting. To this end, we have prepared a broad set of silica rich zeolites and measured their adsorption properties towards two prototypical dipolar fluids: water and methanol. By combining such adsorption measurements with ^{29}Si NMR and IR spectroscopy measurements, we show that for both fluids the non-wetting/wetting crossover observed upon increasing the -OH concentration occurs at the same surface density ~2.5 OH/nm^2. In addition to providing a single critical value for all zeolites, our findings allow generalizing the impact of such defects to other dipolar molecules (i.e. molecules sensitive to such defect types). In

particular, we show that our results provide a means to establish correlations between the vapor uptakes for different hydrophobic zeolites through their dependence on the OH concentration.

RESULTS

We have followed different synthesis approaches to prepare a variety of Si-rich zeolites with different concentrations in hydroxyl groups. Most samples have been synthesized without aluminum sources (e.g all-silica zeolites). For all-silica zeolites, as discussed in the Supporting Information, the synthesis approaches in basic (OH^-) and fluoride media (F^-), which are known to generate different levels of hydrophobicity, have been used [17,29]. Nearly perfect hydrophobic silicalite-1 crystals can be obtained with an extremely low density of internal defects by using fluorine ions as the mineralizing agent at near neutral conditions (instead of the traditional OH- mineralizing agent at alkaline conditions). For parent Aluminum containing-zeolites, post-treatments (e.g. steaming, dealumination by acid/base treatments) have been applied for the removal of Al species, which is supposed to be accompanied by the formation of hydroxyl defects [30]. Two Si rich BEA zeolites with Si/Al= 10 and 18 have been added to complete the zeolite library. In total, 15 zeolite samples – with different structures and/or chemical compositions – have been considered in the present study. Their morphological and chemical compositions together with their adsorption capacity for nitrogen at 77 K and water and methanol at ambient temperature are shown in Table S1 in the Supporting Information. Throughout this manuscript, the different samples will be referred to using the following convention: each sample is assigned a code Xk where X is a number denoting its zeolite framework and k is a letter denoting a synthesis mode. For a few samples, we also indicate by the use of a ’ sign (i.e. Xk’) a variant obtained by a post-treatment process. In practice, as shown in Table 1, X = 1, 2, 3 and 4 refer to silicalite-1, ITQ-13, beta and chabazite zeolites while k corresponds to a, b, c or d.

The N_2 physisorption data at 77 K shown in Figure S3 of the Supporting Information display type I adsorption isotherms with inferred BET surface area matching the expected values for these zeolite structure. A sharp increase in the N_2 uptake for $P/P_0 > 0.95$ can be observed – especially for 1a, 1a’, 3a, 3a’, 3b, 3b’ which can be explained by the small size of the crystal that lead to adsorption at the extra-crystalline surface. In order to avoid porous volume overestimation, pore volumes for the three different probe molecules (N_2, H_2O and MeOH) were assessed from the adsorption capacity at P/P_0 = 0.95. Additional characterization by SEM, IR and ^{29}Si NMR, which are consistent with available data from the literature, can be found in the Supporting Information. The structure of the samples has been checked by Powder X-Ray Diffraction (see Figure S2 in the Supporting Information). A discussion on

the characterization of the type of defects goes beyond of this study and readers are encourage to read literature on this subject [16,18–21].

Table 1. Synthesis routes and adsorption capacities for the different zeolites considered in the present study. The adsorption capacities were assessed using different adsorbate probes: nitrogen at 77 K and water and methanol at ambient temperature.

Code	Synthesis	Name	Si/Al	S BET (m^2/g)	V_{N2}*(cm^3/g)	V_{H2O} (cm^3/g)	V_{MeOH} (cm^3/g)	V_{H2O}/V_{N2}
1a	(OH^-)	silicalite-1	∞	462	0.210	0.080	0.158	0.382
1a'	(OH^-) & NH_4F	silicalite-1	∞	474	0.210	0.061	0.193	0.292
1b	(OH^-) & (F-)	silicalite-1	∞	489	0.190	0.100	0.208	0.526
1c	(OH^-) & (F-)	silicalite-1	∞	503	0.190	0.056	0.174	0.295
1d	(F-)	silicalite-1	∞	382	0.190	0.005	0.087	0.028
2a	(F-)	ITQ-13	∞	358	0.150	0.131	0.145	0.873
2a'	degerm. (F-)	ITQ-13	∞	372	0.150	0.109	0.204	0.727
2b	(F-)	ITQ-13	∞	445	0.170	0.031	0.162	0.184
3a	(OH^-)	Beta	10	588	0.230	0.252	0.271	1.096
3a'	(OH^-) dealum.	Beta	∞	456	0.150	0.205	0.238	1.367
3b	(OH-)	Beta	18	738	0.290	0.271	0.299	0.934
3b'	(OH-) dealum.	Beta	∞	676	0.260	0.303	0.306	1.163
3c	(F^-)	Beta	∞	560	0.230	0.030	0.257	0.131
3c'	(F^-) & steamed	Beta	∞	582	0.230	0.029	0.266	0.127
4a	(F-)	Chabazite	∞	962	0.370	0.117	0.295	0.377

The * indicates that the porous volume was estimated from the adsorbed amount at P/P_0 = 0.90.

Synthesis codes: basic medium (OH-), fluoride medium (F-), degermination process (degerm), dealumination (dealum), steamed

Figures 1 and 2 show for each zeolite sample the water and methanol adsorption isotherms at room temperature, respectively. The data are presented here by structure type: silicalite-1, chabazite and ITQ-13, and beta in panels a, b, and c, respectively. We can classify the isotherms in 3 different groups: Type I isotherms with different slopes, Type V isotherms with the "S" characteristic shapes and lastly rather linear isotherms with low to very low uptake at pressure when approaching P_0.

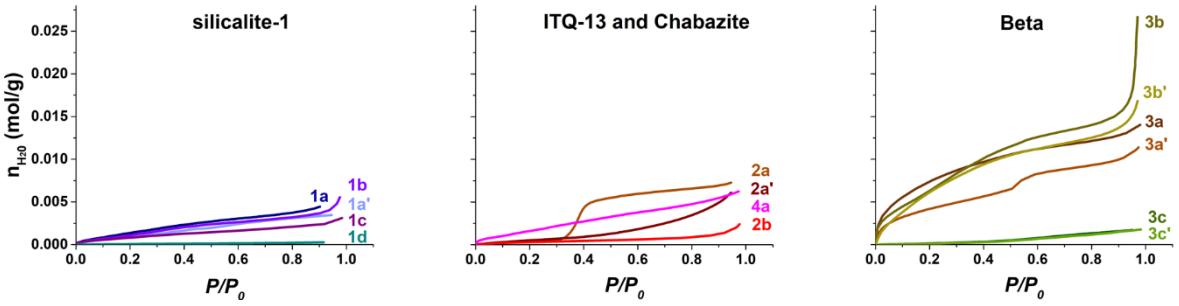

Figure 1. Water adsorption isotherms at 293.15 K for the different zeolite samples. The adsorbed amount is expressed in mol of water per gram of sample. The pressure axis is normalized to the bulk saturating vapor pressure P_0 at the measurement temperature.

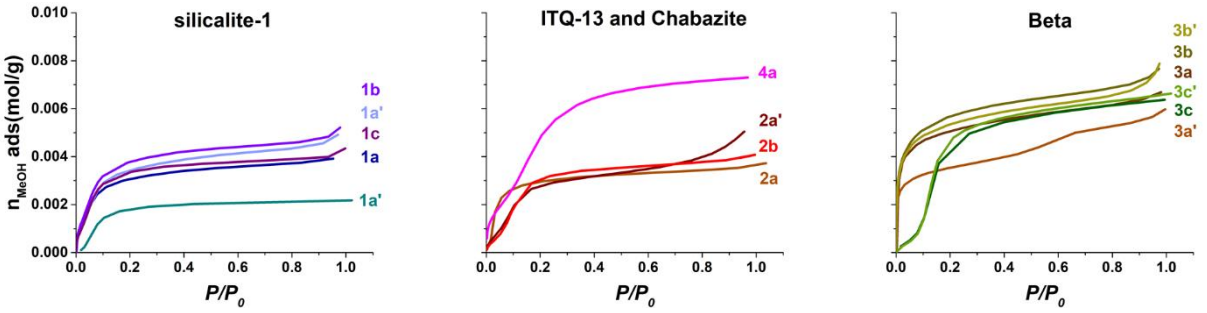

Figure 2. Methanol adsorption isotherms at 293.15 K for the different zeolite samples. The adsorbed amount is expressed in mol of water per gram of sample. The pressure axis is normalized to the bulk saturating vapor pressure P_0 at the measurement temperature.

Fig. 3 compares the pore volumes estimated from the adsorption isotherms for H_2O and MeOH at room temperature with those obtained from the low temperature N_2 adsorption isotherm. The latter being considered as reference data as usually done in the literature (we simply assume that the porous volume seen by N_2 physisorption is the most reliable data owing to the small size for this probe molecule). In all cases, as indicated in Table 1, the porous volumes V_{N2}, V_{H2O} and V_{MeOH} were estimated from the adsorbed amount $n(0.95\ P_0)$ at $P = 0.95\ P_0$ which is then converted into a volume using the liquid density ρ_l^0 of the adsorbate at saturation, i.e. $V = n(0.95\ P_0)/\rho_l^0$. For the 3b sample, the increase in water pressure due to capillary condensation between grains starts before $P/P_0 = 0.95$. In that respect, the porous volume V_{H2O} was taken at $P/P_0 = 0.9$. By plotting in Fig. 3 V_{H2O} and V_{MeOH} as a function of V_{N2}, we aim to check whether or not the data obeyed Gurvich rule stating that adsorbates exploring the same porosity provide the same porous volume when converting adsorbed amounts using the liquid density at saturation. A clear trend appears from the data shown in Fig. 3. The estimated pore volumes using MeOH and N_2 are found to be strongly correlated, therefore suggesting that these two molecules explore the entire porosity for all samples. In contrast, except for a few samples, the data

for water does not correlate with those from nitrogen as the porous volume inferred from water adsorption is about 25% lower that than obtained from nitrogen adsorption. In more detail, owing to the presence aluminum, the samples 3a and 3b are hydrophilic so that V_{H2O} is similar to V_{N2} as water gets adsorbed through their entire porosity. Similarly, despite their large Si/Al ratio (Si/Al $\rightarrow \infty$), the samples 3a' and 3b' are also hydrophilic so that porous volumes inferred from water and nitrogen adsorption are found to be consistent. For those two samples, the hydrophilic character can be attributed to a high density of internal silanols resulting from the dealumination. These data show that water is an appropriate probe for the characterization of hydrophilic surfaces as adsorption for these samples is not governed by fluid/fluid interactions but rather by surface/fluid interactions at low pressure.

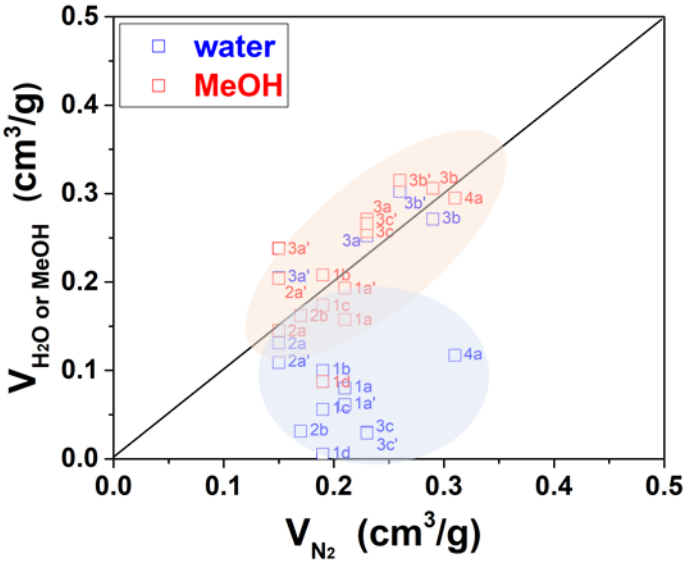

Figure 3. Correlation between the pore volume inferred from water adsorption capacity (blue square) and methanol adsorption capacity (red square) at room temperature and the pore volume estimated by means of nitrogen adsorption at 77 K. For these three adsorbate probes, the pore volume is determined from the adsorbed amount at P/P_0 = 0.95 converted into porous volumes using the bulk liquid density at the corresponding temperature.

Major differences between water and MeOH adsorption uptakes can be observed from the low-pressure range of the adsorption isotherms shown in Figs. 1 and 2. In general, while water uptake is very little on hydrophobic zeolites, MeOH uptake is significant even at low pressure. There are however two exceptions to this general trend; BEA zeolites synthesized in alkaline media (3a, 3a', 3b, 3b') are known to be relatively hydrophilic and ITQ-13 synthesized in fluoride media (2a, 2a'). To provide a quantitative analysis of surface affinity towards each molecular probe, Henry constants K for water and methanol adsorption was determined from the slope of the adsorption isotherms at low pressure

(P/P_0 < 0.1), $n \sim KP$. As shown in Table 2, the Henry constants K for the zeolite set considered here spans over two orders of magnitude; this indicates that K is a well-suited parameter for surface analysis despite the fact that we considered only Si-rich zeolites. From the Henry constants for water adsorption, we can classify the zeolites into 3 categories depending on their hydrophobicity/hydrophilicity: 1 - Very hydrophobic zeolites with $K \sim 15.10^{-7} – 150.10^{-7}$ mol.g^{-1}.Pa^{-1}; these samples are synthesized in fluoride media at the exception of chabazite which is known to show defects despite the fluoride media; 2 - Hydrophobic zeolites $K \sim 150.10^{-7} – 3300.10^{-7}$ mol.g^{-1}.Pa^{-1}; these samples correspond to silicalite-1 zeolites synthesized in basic media and chabazite synthesized in fluoride media and 3- Less hydrophobic zeolites with $K \sim 3300.10^{-7} – 4500.10^{-7}$ mol.g^{-1}.Pa^{-1}; these samples correspond to beta zeolites synthesized in basic media (regardless post-treatment).

Table 2. Number or density of OH groups in the considered zeolite structures as determined by ^{29}Si NMR and infrared spectroscopy. The water and methanol Henry constants as calculated from the slope of the adsorption isotherms in the low-pressure range. Such Henry constants are given in 10^7 mol.g^{-1}.Pa^{-1}. The *K'* notation corresponds to the normalized Henry constant by saturation vapor pressure of water or MeOH at 293.15 K.

Code	OH_{IR} (a.u)	$[OH]_{NMR}$ /nm^2	K_{water}	K_{MeOH}	K'_{MeOH}/K'_{water}
1a	71.8	4.5	2900	520	0.96
1a'	51.4	1 .5	1400	650	2.48
1b	46.3	2.3	825	1140	7.39
1c	36.4	2.0	525	1360	13.85
1d	18.3	0.3	15	100	35.65
2a	37.4	n.m.	75	530	37.79
2a'	39.1	3.1	150	230	8.20
2b	20.0	4.4	45	100	11.88
3a	112.5	n.m.	3900	3000	3.98
3a'	161.2	14.6	4500	6500	7.72
3b	77.2	n.m.	2770	3160	6.10
3b'	104.6	9.2	4050	3680	4.86
3c	32.6	0.8	23	70	16.64
3c'	22.6	0.5	30	80	14.26
4a	82.0	3.9	3300	1260	2.04

n.m. Not measured. The concentration of OH for 2a, 3a and 3b cannot be measured by Si NMR as these two solids contain Al, unlike other solids.

For silicalite-1 (1a) and BEA (3a, 3a', 3b, 3b') zeolites obtained in alkaline media, the concentrations of Q^3 silanols per nm^2 are relatively high when comparing to others and in good agreement with literature data [22,33]. The low intensity of Q^3 signals for zeolites prepared in fluoride media can make hard the accurate estimation of the silanol concentration – especially for 1d, 3c and 3c' zeolites for which concentrations are below $1/nm^2$. In order to check the estimation of OH concentration, especially for low concentration, a semi-quantitative analysis of hydroxyl groups was carried by means of Diffuse Reflectance Infrared Fourier Transform Spectroscopy (DRIFTS) for all solids. Typical DRIFTS spectra for the beta and silicalite-1 zeolites are shown in Fig. 4. The signal from ~3800 to ~3000 cm^{-1}, which corresponds to vibration modes of free and H-bonded hydroxyls, were integrated and corrected for the two following effects (see supplementary information for full detail: Figures S6 and S7). First, the OH band areas were divided by the area of the overtone signal corresponding to zeolite framework (1800-2100 cm^{-1}), therefore leading to a signal normalized to the sample mass. Thereafter, these concentrations are labelled "normalized hydroxyl numbers" in arbitrary units OH_{IR} (a.u) as shown Table 2.

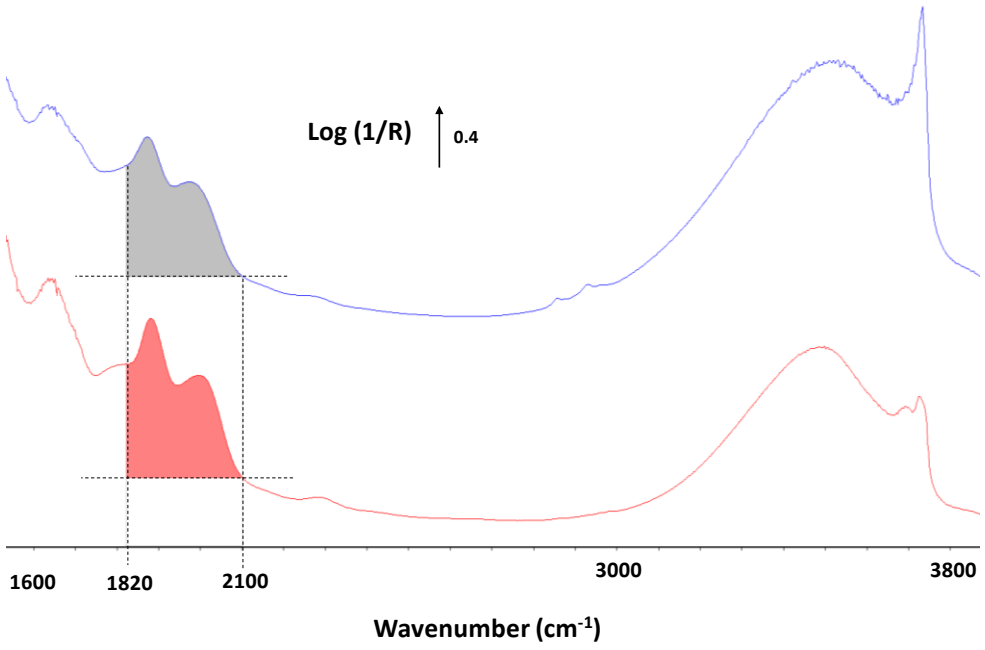

Figure 4. DRIFTS spectra of 1b (bottom) and (3b') zeolite showing the integration boundaries of zeolite overtone (1800-2100 cm^{-1}) and hydroxyl stretching vibrations (3000-3800 cm^{-1}). The spectra were offset for the sake of clarity.

The silanol concentrations as measured by ^{29}Si NMR are compared with the normalized hydroxyl numbers as determined by DRIFTS (Fig. 5). We observe a strong correlation between these two

analytical methods even if they probe different species. Indeed, whereas NMR is sensitive to the Si atom environment, DRIFTS is sensitive to O-H vibrations. Importantly, we can observe that low OH concentrations as determined by ^{29}Si NMR (samples 1d, 3c and 3c') do not deviate from the linear correlation which confirm the validity of ^{29}Si NMR for almost defect free all-silica zeolites. The zeolite ITQ-13 prepared in fluoride media (sample 2b) is obviously an outlier. We believe that this departure is due to the presence of an amorphous phase in this zeolite structure (as suggested by the XRD data shown in the Supporting Information: Figure 2).

Having this linear correlation in hands, it allows an estimation of silanol concentration for Ge- and Al-containing zeolites. For 2a, 3a, and 3b zeolites, the silanol concentration could not be determined by means of ^{29}Si NMR spectroscopy due to the presence of Germanium or Aluminium atoms in the structure. Therefore, to overcome this issue, the silanol concentration for these samples – 2.13, 8.95, and 5.77 Si-OH per nm^2, respectively – was estimated from their normalized hydroxyl numbers determined by DRIFT using the linear correlation between hydroxyl numbers (DRIFTS) and the Q^3 silanol concentration (^{29}Si NMR) observed for the other samples and used as calibration method.

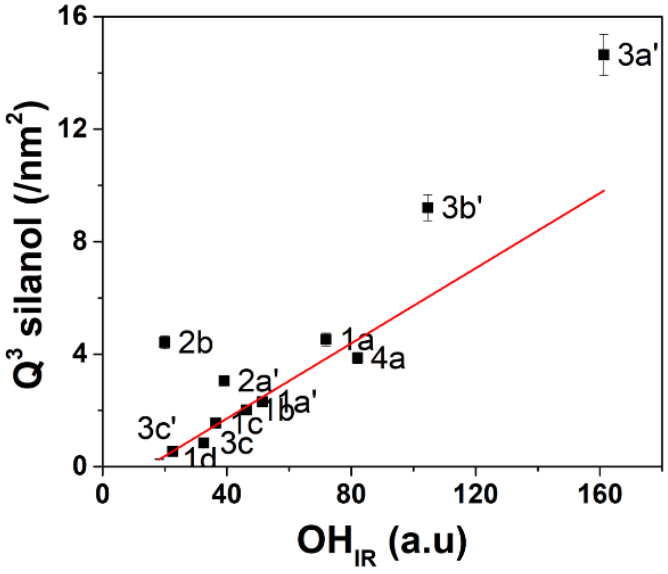

Figure 5. Correlation between hydroxyl concentrations as determined by DRIFTS and the concentration of Q^3 silanol measured by ^{29}Si NMR for Si-rich zeolites as labelled in in the figure (see Table 1 or Table 2 for the labelling code). The red line shows a linear regression fit of the data. The error bar, which is indicated for each datapoint, is smaller than the symbol size for some samples.

To assess the impact of silanol concentration on surface interactions, we plot the Henry constants *K* for water and MeOH adsorption as a function of the silanol defect concentration for each zeolite

considered in this study. The main figure (Fig. 6) shows the data obtained for the entire zeolite library while the insert shows a zoom in the low defect concentration region. Regardless of the probe molecule (i.e. water or methanol), two major trends can be noted. First, the Henry constants *K* are very low for silanol concentrations < 2.5 OH nm^2 while *K* increases with the silanol concentration for silanol concentrations > 2.5/nm^2. Typically, *K* is of the order of 10^{-6} mol.g^{-1}.Pa^{-1} for low silanol concentrations while it increases from ~10^{-6} to ~10^{-5} mol.g^{-1}.Pa^{-1} for higher silanol concentrations. Second, the Henry constants (*K)* for water are smaller than those for methanol when the silanol concentration is below 2.5/nm^2 while the opposite trend is observed when the silanol concentration > 2.5/nm^2 . These data suggest that the critical silanol concentration around ~2.5 per nm^2 drives the adsorption of polar substrates in Si-rich zeolites.

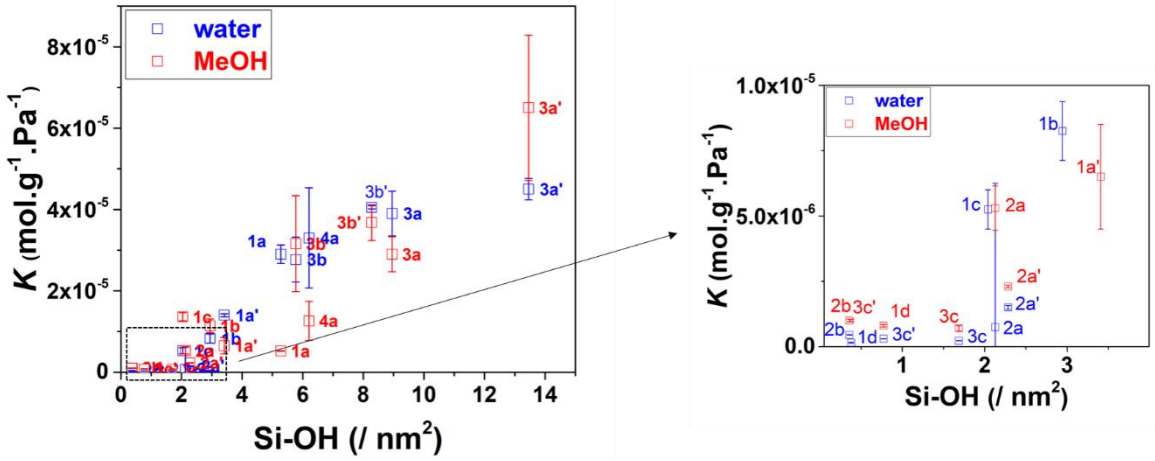

Figure 6. Correlation between the number of Si-OH per nm^2 and the Henry constants for water and MeOH adsorption (the blue and red data are for water and methanol, respectively). The insert shows a zoom on low silanol concentration range.

DISCUSSION

The shape for each single isotherm including hysteresis between adsorption and desorption branches can be interpreted as follows (see also Figure S4 and S5 in Supplementary Information). As expected for zeolite materials, all N_2 adsorption isotherms at 77 K are characteristic of microporous materials. In particular, the adsorbed amount increases strongly in the low pressure range as N_2 gets adsorbed in the very narrow porosity in the subnanometer/nanometer range. Moreover, depending on the mesoporosity available in the samples, which mostly corresponds to the volume available between the zeolite grains, a sharp increase in the adsorbed amount at pressures above 0.8 P_0 is observed[31]. Such an increase corresponds to capillary condensation within the mesopores as further confirmed in some cases by the fact that desorption shows a hysteresis loop (for a discussion on the hysteresis loop

observed for large pores but absent for small pores, the reader is referred to [32]). In contrast to nitrogen adsorption, the data for methanol and water adsorption displays behaviors that drastically depend on the silanol surface density. For water adsorption, while the adsorbed amount increases strongly at low pressure for large silanol densities, the adsorbed amount increases only very weakly and in a linear fashion for small silanol densities. In particular, for some intermediate silanol densities (see sample 2a), a hybrid wetting situation is observed as only little water adsorption is observed at low pressures while rapid pore filling occurs at moderate pressures around 0.4 P_0. Overall, the same transition between non-wetting or weakly wetting to wetting situations is observed for methanol upon increasing the silanol surface density. However, as expected, for a given sample, due to its weaker interactions with the surface compared to water, the adsorption of methanol is always more favorable than that of water.

The structural silanol defects (SiOH) consist of terminating silanol groups in the Si–O–Si network where oxygen atoms are not bonded to two silicon atoms or form internal silanol groups where the Si–O–Si bonds are broken. In the latter case, it is also possible that silicon or aluminum atoms detach from the zeolite framework during synthesis so that a maximum of four silanol groups can be accordingly formed per each missing silicon atom; this structure is coined as 'silanol nest'. The concentration and types of silanol defects – either distributed in the structure or localized as 'nest' or "patches" – are the two key aspect which governs the condensation mechanism for water and possibly for other polar adsorbates on overall hydrophobic Si-rich zeolites [13, 16, 17, 19]. The DRIFTS and ^{29}Si NMR techniques used in this study are not spatially resolved so that we cannot determine whether the silanol defects are homogeneously distributed in the crystals or localized at specific sites. Yet, the combination of these two powerful techniques provides an overall assessment of the silanol defect concentration. As far as DRIFTS is concerned, it allows semi quantitative analysis of hydroxyl numbers for Al- or Ge- containing zeolites. Also the higher sensitivity of this technique to hydroxyl signals makes this technique very relevant for the quantification of low defective Si-rich zeolites. On the other hand, DRIFTS does not provide quantitative concentrations as the optical path in such measurements is unknown in most cases (unless calibration curves or relevant absorption coefficients are available for both zeolite overtones and hydroxyls). As for ^{29}Si NMR, this method provides silanol defect concentration per unit cell which can be readily converted per surface area. Yet, it cannot be applied to Al- Ge containing zeolites. Also, it is not very sensitive to low silanol concentration, therefore making it less appropriate for low defect zeolites. However, as shown in this paper for a large variety of silica-rich zeolites, the strong correlation observed between DRIFT and ^{29}Si NMR silanol assessment provides a cross-validation between these two techniques. Such a linear correlation, despite its empirical nature, enables accurate quantification of the overall surface silanol concentration through the integration of

the hydroxyl signals obtained by DRIFT – even for Ge- and Al-containing zeolites and very weakly defective silica-rich zeolites.

Our data obtained using this two strategies approach suggest that the silanol concentration of 2.5 SiOH/nm^2 plays a pivotal role in the adsorption properties of Si-rich zeolites. As shown in this paper, at this specific concentration, a crossover is observed in both water and methanol adsorption. While zeolites with lower silanol concentrations hardly adsorb neither water nor methanol, the adsorbate-surface interaction (as probed through the Henry constant in the low pressure range) increases linearly with the silanol concentration beyond this critical concentration. Moreover, this critical silanol concentration of 2.5 OH/nm^2 is also discriminant for hydrophobic zeolites when looking at MeOH/water ideal selectivity; indeed, there is a clear selectivity transition in the region around 3 OH/nm^2 (Fig. 7). For lower silanol defects, the separation factor at isopressure – as inferred from the Henry constant ratio for MeOH/water –is above 30, therefore indicating a very selective behavior towards MeOH. On the other hand, for larger defect concentration, the zeolites are not hydrophobic enough to be selective towards MeOH.

Finally, we note that the existence of a silanol concentration is consistent with available microscopic studies on water adsorption in Si-rich zeolites. The mechanism of water condensation in hydrophobic zeolites – especially all silica zeolites – was studied by means of Grand Canonical molecular simulations. Fuchs and coworkers [13,34] reported the impact of silanol patches on water adsorption in silicalite-1 which modifies its adsorption properties. Similarly, [28] Ahunbay et al. studied water adsorption on silicalite-1 with different amount of “nest” defects (4 adjacent Si-OH) and found that the existence of 0.125 silanol nest per unit cell increases the heat of adsorption for water at low coverage. As far as the surface silanol density is concerned, we note that Siboulet et al. [35,36] observed for an amorphous silica surface a hydrophobic to hydrophilic transition located between 0 and 3.7 OH nm^{-2} (such a crossover was observed either by monitoring the shift in capillary condensation or hydrodynamics slippage at the pore surface).

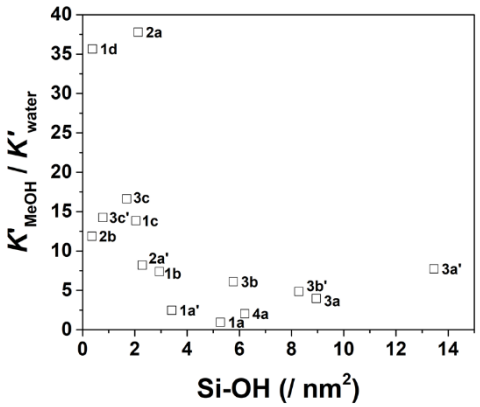

Figure 7. Correlation between the number of silanol per nm^2 and the ratio of Henry's constants showing the selectivity of zeolites towards water and MeOH

Conclusions.

Despite this abundant theoretical literature, the establishment of a robust experimental correlation between silanol defect concentration in zeolites and water adsorption was still lacking. The present work is an important step in this direction as we have reported important data showing the existence of a critical silanol concentration at 2.5 OH/nm^2 inducing a crossover in the adsorption properties not only for water, but also for methanol. While this parameter does not take into account the microscopic nature of silanol defects, it constitutes a strong descriptor as it seems to govern adsorption for polar substrates, such water and methanol in silica-rich zeolites.

Supporting informations.

Zeolite synthesis procedures; NMR spectra; XRD patterns; N_2, water and MeOH adsorption-desorption isotherms; DRIFTS spectra; electronic microscopy pictures are available in the supporting information file.

Acknowledgments.

This study has received funding from the European Union's Horizon 2020 research and innovation program, IMPRESS under grant agreement No 869993 and from French National Research Agency (ANR), CATCALL (ANR-19-CE07-0025)

References

(1) Gläser, R.; Roesky, R.; Boger, T.; Eigenberger, G.; Ernst, S.; Weitkamp, J. Probing the Hydrophobic Properties of MCM-41-Type Materials by the Hydrophobicity Index. *Progress in Zeolite And Microporous Mater. PTS A-C*, **1997**, *105*, 695–702.

(2) Ng, E.-P.; Mintova, S. Nanoporous Materials with Enhanced Hydrophilicity and High Water Sorption Capacity. *Microporous Mesoporous Mater.* **2008**, *114*, 1–26.

(3) Giovambattista, N.; Rossky, P. J.; Debenedetti, P. G. Effect of Pressure on the Phase Behavior and Structure of Water Confined between Nanoscale Hydrophobic and Hydrophilic Plates. *Phys. Rev. E* **2006**, *73*, 041604.

(4) Eroshenko, V.; Regis, R.-C.; Soulard, M.; Patarin, J. Les systèmes hétérogènes « eau–zéolithe hydrophobe »: de nouveaux ressorts moléculaires. *Comptes Rendus Phys.* **2002**, *3*, 111–119.

(5) Soulard, M.; Patarin, J.; Eroshenko, V.; Regis, R. Molecular Spring or Bumper: A New Application for Hydrophobic Zeolitic Materials. *Recent Advances in The Science and Technology of Zeolites and Related Materials, PTS A - C*, 2004, *154*, 1830–1837.

(6) Farzaneh, A.; DeJaco, R. F.; Ohlin, L.; Holmgren, A.; Siepmann, J. I.; Grahn, M. Comparative Study of the Effect of Defects on Selective Adsorption of Butanol from Butanol/Water Binary Vapor Mixtures in Silicalite-1 Films. *Langmuir* **2017**, *33*, 8420–8427.

(7) Gravelle, S.; Yoshida, H.; Joly, L.; Ybert, C.; Bocquet, L. Carbon Membranes for Efficient Water-Ethanol Separation. *J. Chem. Phys.* **2016**, *145*, 124708.

(8) Jiang, N.; Shang, R.; Heijman, S. G. J.; Rietveld, L. C. High-Silica Zeolites for Adsorption of Organic Micro-Pollutants in Water Treatment: A Review. *Water Res.* **2018**, *144*, 145–161.

(9) Cosseron, A.-F.; Daou, T. J.; Tzanis, L.; Nouali, H.; Deroche, I.; Coasne, B.; Tchamber, V. Adsorption of Volatile Organic Compounds in Pure Silica CHA, ∗BEA, MFI and STT-Type Zeolites. *Microporous Mesoporous Mater.* **2013**, *173*, 147–154.

(10) Jin, H.; Jiang, N.; Oh, S.-M.; Park, S.-E. Epoxidation of Linear Olefins over Stacked TS-1 Zeolite Catalysts. *Top. Catal.* **2009**, *52*, 169–177.

(11) Trzpit, M.; Soulard, M.; Patarin, J.; Desbiens, N.; Cailliez, F.; Boutin, A.; Demachy, I.; Fuchs, A. H. The Effect of Local Defects on Water Adsorption in Silicalite-1 Zeolite: A Joint Experimental and Molecular Simulation Study. *Langmuir* **2007**, *23*, 10131–10139.

(12) Bolis, V.; Busco, C.; Ugliengo, P. Thermodynamic Study of Water Adsorption in High-Silica Zeolites. *J. Phys. Chem. B* **2006**, *110*, 14849–14859.

(13) Desbiens, N.; Demachy, I.; Fuchs, A. H.; Kirsch-Rodeschini, H.; Soulard, M.; Patarin, J. Water Condensation in Hydrophobic Nanopores. *Angew. Chem. Int. Ed.* **2005**, *44*, 5310–5313.

(14) Deroche, I.; Daou, T. J.; Picard, C.; Coasne, B. Reminiscent Capillarity in Subnanopores. *Nat. Commun.* **2019**, *10*, 4642.

(15) Coasne, B.; Gubbins, K. E.; Pellenq, R. J.-M. Temperature Effect on Adsorption/Desorption Isotherms for a Simple Fluid Confined within Various Nanopores. *Adsorption* **2005**, *11*,

(16) Senderov, E.; Halasz, I.; Olson, D. H. On Existence of Hydroxyl Nests in Acid Dealuminated Zeolite Y. *Microporous Mesoporous Mater.* **2014**, *186*, 94–100.

(17) Zhang, K.; Lively, R. P.; Noel, J. D.; Dose, M. E.; McCool, B. A.; Chance, R. R.; Koros, W. J. Adsorption of Water and Ethanol in MFI-Type Zeolites. *Langmuir* **2012**, *28*, 8664–8673.

(18) Zecchina, A.; Bordiga, S.; Spoto, G.; Marchese, L.; Petrini, G.; Leofanti, G.; Padovan, M. Silicalite Characterization. 1. Structure, Adsorptive Capacity, and IR Spectroscopy of the Framework and Hydroxyl Modes. *J. Phys. Chem.* **1992**, *96*, 4985–4990.

(19) Bordiga, S.; Roggero, I.; Ugliengo, P.; Zecchina, A.; Bolis, V.; Artioli, G.; Buzzoni, R.; Marra, G.; Rivetti, F.; Spanò, G.; Lamberti, C. Characterisation of Defective Silicalites. *J. Chem. Soc. Dalton Trans.* **2000**, 21, 3921–3929.

(20) Dessau, R.; Schmitt, K.; Kerr, G.; Woolery, G.; Alemany, L. On the proposed clustering of silanol groups in ZSM-5. *J. Catal.* **1988**, *109*, 472–473.

(21) Koller, H.; Lobo, R. F.; Burkett, S. L.; Davis, M. E. SiO-HOSi Hydrogen Bonds in As-Synthesized High-Silica Zeolites. *J. Phys. Chem.* **1995**, *99*, 12588–12596.

(22) Burel, L.; Tuel, A. Nanozeolites: New Strategies for Designing Ultra Small Silicalite Crystals with Very Few Framework Defects. *Microporous Mesoporous Mater.* **2013**, *174*, 90–99.

(23) Axon, S. A.; Klinowski, J. Synthesis and Characterization of Defect-Free Crystals of MFI-Type Zeolites. *Appl. Catal. Gen.* **1992**, *81*, 27–34.

(24) Caullet, P.; Paillaud, J.-L.; Simon-Masseron, A.; Soulard, M.; Patarin, J. The Fluoride Route: A Strategy to Crystalline Porous Materials. *Comptes Rendus Chim.* **2005**, *8*, 245–266.

(25) Guth, J. L.; Delmotte, L.; Soulard, M.; Brunard, N.; Joly, J. F.; Espinat, D. Synthesis of AI,Si-MFI-Type Zeolites in the Presence of F- Anions: Structural and Physicochemical Characteristics. *Zeolites* **1992**, 12, 929-935

(26) Camblor, M. A.; Corma, A.; Valencia, S. Synthesis in Fluoride Media and Characterisation of Aluminosilicate Zeolite Beta. *J. Mater. Chem.* **1998**, *8*, 2137–2145.

(27) Gläser, R.; Weitkamp, J. Surface Hydrophobicity or Hydrophilicity of Porous Solids. In *Handbook of Porous Solids*; Germany, Schth, F., Sing, K. S. W., Weitkamp, J., Eds.; Wiley-VCH Verlag GmbH: Weinheim, 2002, 395–431.

(28) Ahunbay, M. G. Monte Carlo Simulation of Water Adsorption in Hydrophobic MFI Zeolites with Hydrophilic Sites. *Langmuir* **2011**, *27*, 4986–4993.

(29) Chezeau, J. M.; Delmotte, L.; Guth, J. L.; Gabelica, Z. Influence of Synthesis Conditions and Postsynthesis Treatments on the Nature and Quantity of Structural Defects in Highly Siliceous MFI Zeolites: A High-Resolution Solid-State 29Si n.m.r. Study. *Zeolites* **1991**, *11*, 598–606.

(30) Karge, H. G.; Anderson, P.; Weitkamp, J.; Beyer, H. K.; Gallezot, P.; Harjula, R.; Karge, H. G.; Rymsa, U.; Schulz-Ekloff, G.; Townsend, R. P.; et al. *Post-Synthesis Modification I*; Molecular Sieves; Springer Berlin Heidelberg, 2002.

(31) Coasne, B.; Galarneau, A.; Gerardin, C.; Fajula, F.; Villemot, F. Molecular Simulation of Adsorption and Transport in Hierarchical Porous Materials. *Langmuir* **2013**, *29*, 7864–7875.

(32) Coasne, B. Multiscale Adsorption and Transport in Hierarchical Porous Materials. *New J. Chem.* **2016**, *40*, 4078–4094.

(33) Dzwigaj, S.; Millot, Y.; Che, M. Ta(V)-Single Site BEA Zeolite by Two-Step Postsynthesis Method: Preparation and Characterization. *Catal. Lett.* **2010**, *135*, 169–174.

(34) Desbiens, N.; Boutin, A.; Demachy, I. Water Condensation in Hydrophobic Silicalite-1 Zeolite: A Molecular Simulation Study. *J. Phys. Chem. B* **2005**, *109*, 24071–24076.

(35) Siboulet, B.; Coasne, B.; Dufrêche, J.-F.; Turq, P. Hydrophobic Transition in Porous Amorphous Silica. *J. Phys. Chem. B* **2011**, *115*, 7881–7886.

(36) Siboulet, B.; Molina, J.; Coasne, B.; Turq, P.; Dufreche, J.-F. Water Self-Diffusion at the Surface of Silica Glasses: Effect of Hydrophilic to Hydrophobic Transition. *Mol. Phys.* 2013, *111*, 3410–3417.

TOC